Insights in Photocatalytic/Fenton-based Degradation of Microplastics using Iron-Modified Titanium Dioxide Aerogel Powders

Guru Karthikeyan Thirunavukkarasu[a], Monika Motlochová[a], Dmytro Bavol[a],Anna Vykydalová[a], Jaroslav Kupčík[a], Michal Navrátil[a], Kaplan Kirakci[a], Eva Pližingrová[a], Dana Dvoranová[b], Jan Šubrt[a]*

[a] Institute of Inorganic Chemistry of the Czech Academy of Sciences, Husinec-Řež 250 68, Czech Republic

[b] *Institute of Physical Chemistry and Chemical Physics, Faculty of Chemical and Food Technology, Slovak University of Technology in Bratislava, Bratislava, SK-812 37, Slovak Republic*

*corresponding author: thirunavukkarasu@iic.cas.cz

S2. Materials and Methods

S2.1 High-performance liquid chromatography (HPLC) – High-resolution mass spectrometry (HRMS) analysis

A Vanquish Core High-Performance Liquid Chromatography (HPLC) system equipped with a Diode Array detector (DAD) and further connected to an Orbitrap Exploris™ 120 mass spectrometer was used to separate and identify the newly formed degradation products from PS MPs. Chromatographic conditions were as follows: Kinetex C18 100 Å column (2.6 µm, 150 x 2.1 mm *I.D.*) at 40 °C; flow rate, 0.2 mL/min; detection, DAD (190–800 nm). Separations were performed using a binary gradient based on water (A) and methanol (B), both containing 2.5 mM ammonium acetate. The gradient elution program was the following: 0 – 2 min isocratic at 60% (*v/v*) solvent B; 2 – 13 min liner from 60% to 100% (*v/v*) solvent B; 13 – 15 min isocratic at 100% (*v/v*) solvent B; 15 – 16 min linear from 100% to 60% (*v/v*) solvent B, followed by 8 min equilibration time. The injection volume of all samples was 2 µL.

High-Resolution Mass Spectrometry (HRMS) measurements were performed with a HESI probe (Heated Electrospray Ionization) in negative mode using nitrogen (4.8 Air Products) as a collision gas. Conditions used for the ESI interface: vaporizer temperature 40 °C; N_2 (isolated from air in Genius XE35, Peak Scientific) as a nebulizing sheath gas and auxiliary gas, flow 50 arb. and 15 arb., respectively; spray voltage 3.5 kV; ion transfer tube temperature 320 °C; RF lens 70% and mass range from 60 to 900.

S2.2 Electron paramagnetic resonance (EPR) spectroscopy

The indirect techniques of electron paramagnetic resonance (EPR) spectroscopy were used to detect and identify the generated transient paramagnetic intermediates. Spin trapping agent 5,5-dimethyl-1-pyrroline N-oxide (DMPO) purchased from Sigma-Aldrich was distilled before application, 4-oxo-2,2,6,6-tetramethylpiperidine (TMPO) was purchased from Sigma-Aldrich and hydrogen peroxide (35 %, p. a.) was from CentralChem. The dispersions for EPR experiments

were prepared in deionized water or dimethylsulfoxide (>99.9% DMSO, anhydrous, Sigma-Aldrich) and the measurements were carried out at room temperature (295 K) under air employing an EPR spectrometer EMXPlus (Bruker, Germany) operating at 100 kHz field modulation using the high sensitivity probe-head with the small quartz flat cell (WG 808-Q, Wilmad-LabGlass, optical cell length 0.045 cm). The reaction systems containing $TiAP_{0.1Fe}$ with the other components were prepared directly before measurement and aerated using a gentle airstream before the experiment. The systems were irradiated at 295 K directly in the EPR high-sensitivity resonator, and the EPR spectra were recorded *in situ*. The value of the UVA irradiance (LED@365 nm), determined using a UVX radiometer (UVP, USA) within the EPR cavity, was 17 mW cm^{-2}. All EPR experiments were performed at least in duplicate. EPR spectra acquisition started 2 minutes after experimental system mixing. The experimental EPR spectra were analyzed using WinEPR software (Bruker), while the calculations of spin-Hamiltonian parameters and relative concentrations of individual spin-adducts were performed with the EasySpin toolbox working on the MatLab® platform [1].

Table S1: Calculated CI and PI for all the tested samples are tabulated. The relative change in CI and PI are calculated from these values. Error is ± 5%

Sample	CI	PI
Polystyrene	0.203628	0.540335
Polystyrene_Photolysis with H_2O_2	0.197719	0.65675
TiAP (Before Treatment)	0.233459	0.291411
TiAP_After PC	0.294528	0.179092
TiAP_with H_2O_2	0.353719	0.401656
$TiAP_{0.01Fe}$ (Before Treatment)	0.243922	0.396147
$TiAP_{0.01Fe}$_After PC	0.219978	0.541111
$TiAP_{0.01Fe}$_After PF	0.22116	0.416171
$TiAP_{0.1Fe}$ (Before Treatment)	0.214058	0.380031
$TiAP_{0.1Fe}$_After PC	0.292623	0.307828
$TiAP_{0.1Fe}$_After PF	0.254409	0.601253
$TiAP_{1Fe}$ (Before Treatment)	0.266709	0.432011
$TiAP_{1Fe}$ _After PC	0.243109	0.581313
$TiAP_{1Fe}$ _After PF	0.260957	0.535786

Table S2: Comparison of change in carbonyl and peroxyl indexes with respect to photocatalyst concentration, MPs concentration, irradiation time, and intensity reported in the literature with the current work.

Sample	Photocatalyst Conc. (g/L)	MPs Conc. (g/L)	Irradiation Time	Intensity	Catalyst *vs* Pollutant Ratio	Indexes	Mineralization (%)	Ref
TiAP_With H_2O_2	0.2	0.1	480 min	UVA (Flux density 6.24 mW/cm^2)	2	CI: 0.353 PI: 0.401	53% (after 24 h)	Our Work
TiO_2-P25	1	0.1	240 min	60 W/m^2 (UVA light)	10	Relative CI: 6.5 Relative PI: 2 (calculated after 4 h)	87.5% (after 50 h)	[2]
TiO_2/M (Nanotube Arrays)	-	9	50 h	0.021 mW/cm^2 (at working distance)	-	CI: 0.275	13%	[3]
FeB/TiO_2	1.66	1	12 h	5 W (365 nm LED lamp)	1.66	CI: 3.2	-	[4]
BiOI-Fe_3O_4	0.5	0.05	120 h	50 W (visible light, 400-800 nm)	10	-	23%	[5]
20% P25 in PS film	-	-	500 h	300 W UVB	0.25	CI: 0.8	-	[6]

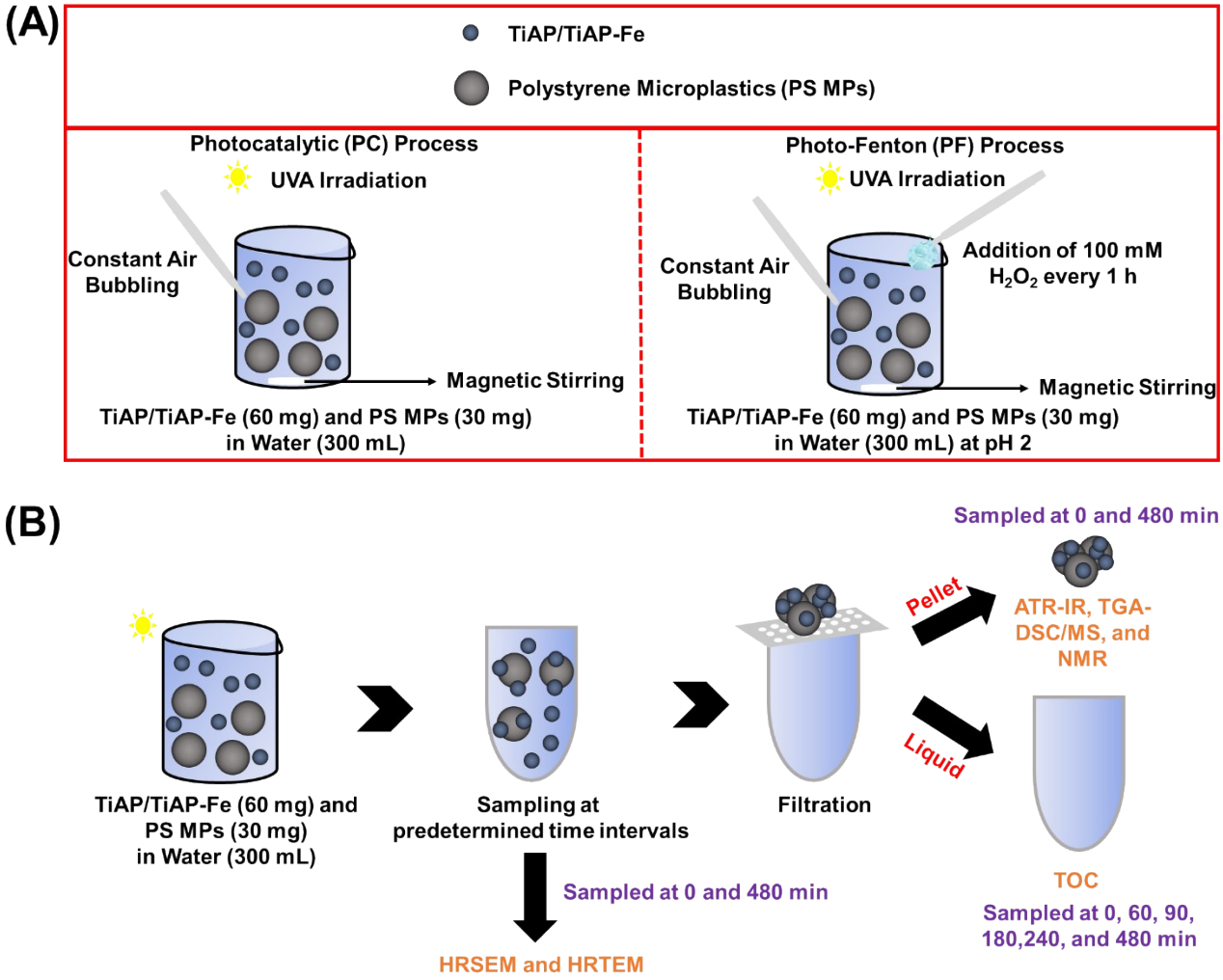

Figure S1: Schematic (A) photocatalytic (PC) and photo-Fenton (PF) process setup and (B) sampling methodologies for evaluating the degradation of PS MPs after the PC and PF processes.

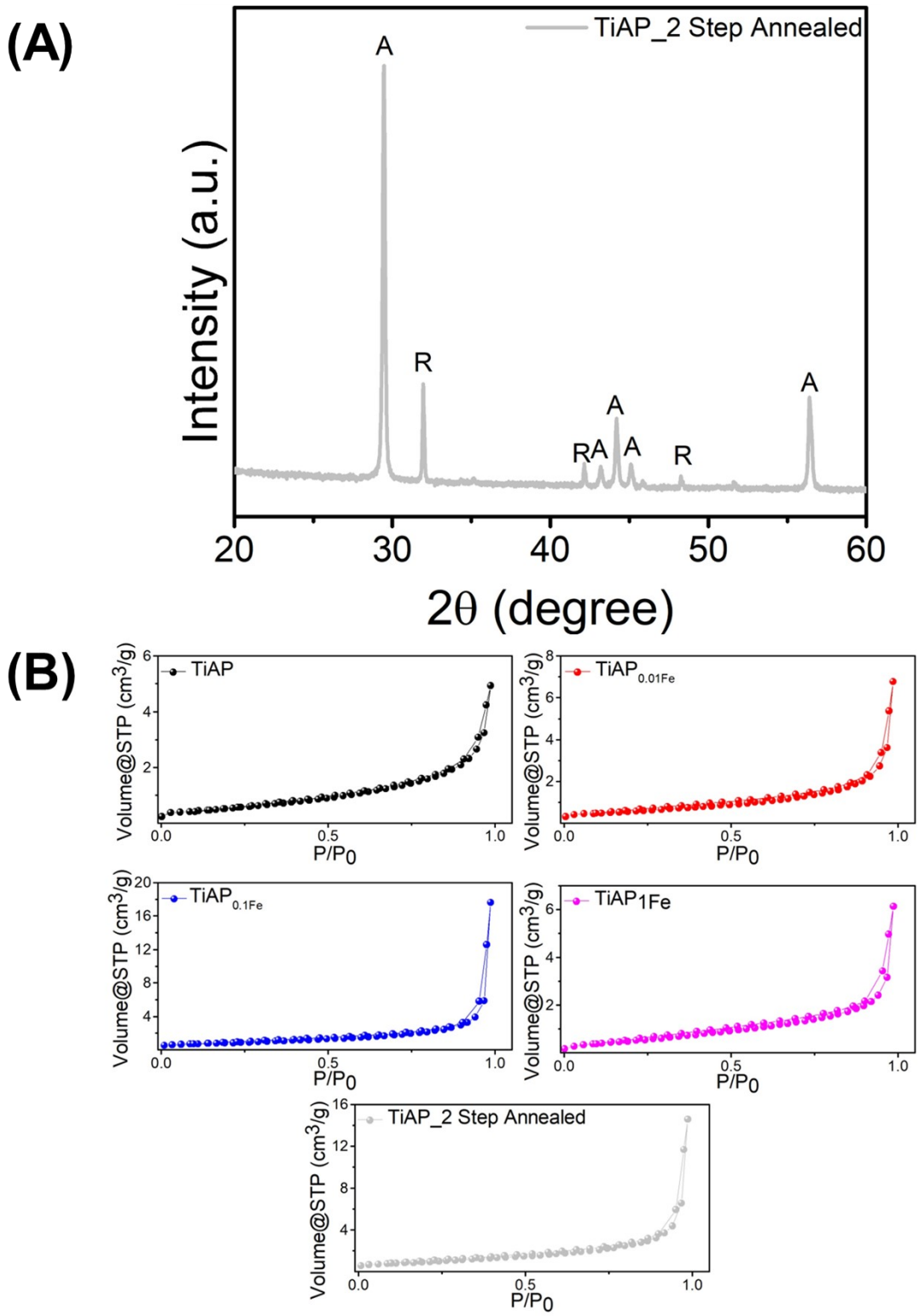

Figure S2: (A) XRD pattern of two-step annealed TiAP and BET adsorption-desorption isotherm of TiAP, all concentrations of Fe-modified TiAP, and two-step annealed TiAP, respectively.

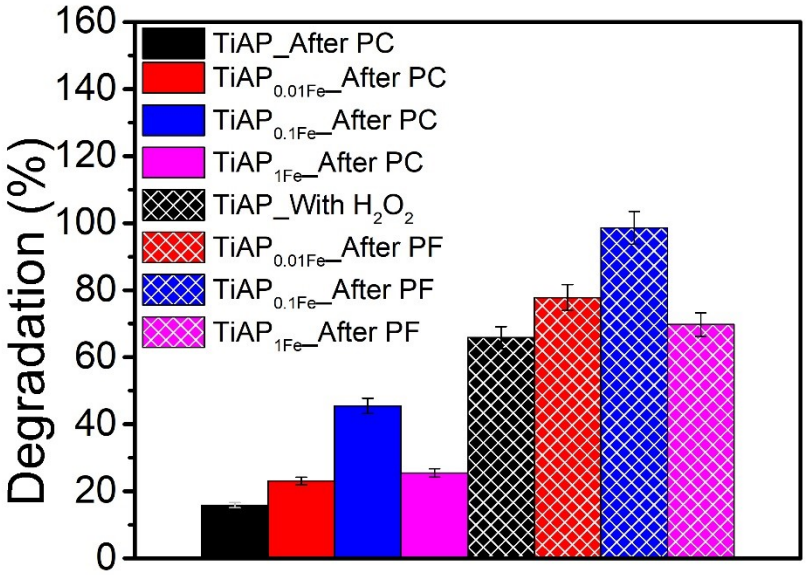

Figure S3: Photocatalytic (PC) and photo-Fenton (PF) processes-based degradation extent of caffeine using TiAP and Fe-modified TiAP (photocatalyst: 0.2 mg/mL, volume: 30 mL, caffeine: 20 ppm, pH 3 and PF process: pH 3, 0.1 mM H_2O_2, irradiation time: 2 h).

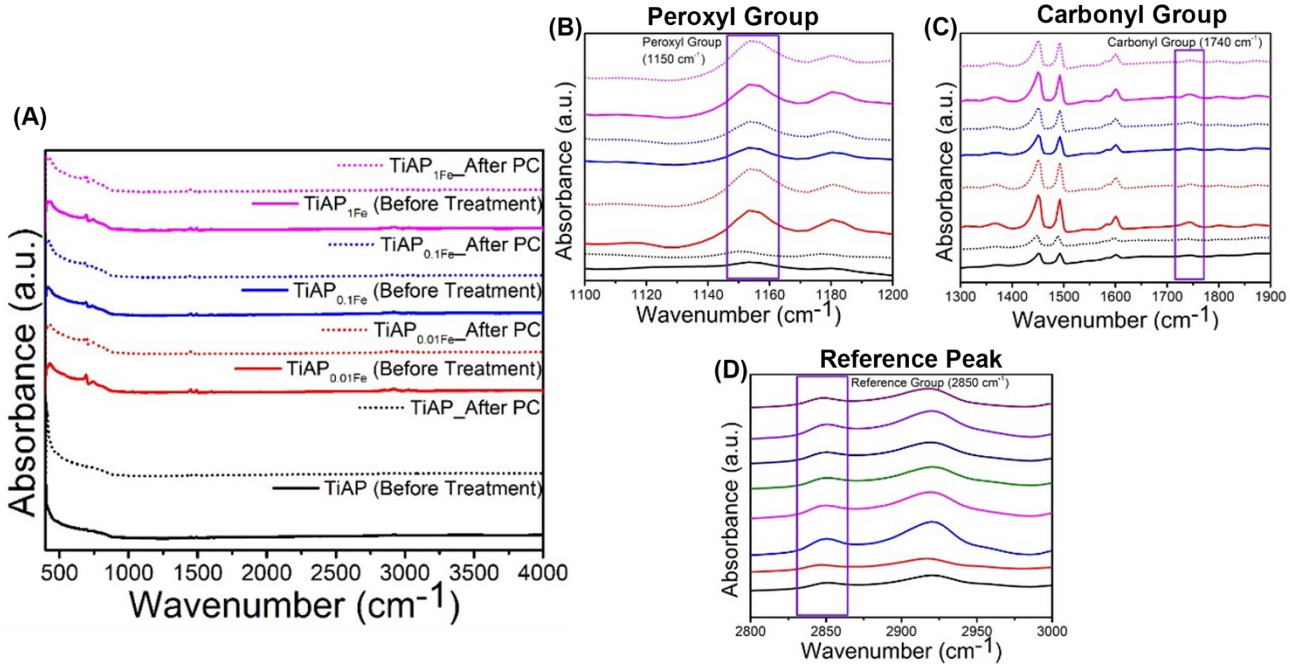

Figure S4: (A) Changes in ATR-IR spectra before (0 min) and after (480 min) the photocatalytic (PC) process for the TiAP and different concentrations of iron-modified TiAP. On the right side, zoomed-in spectra of the peroxyl group (B), carbonyl group (C), and reference group (D), respectively.

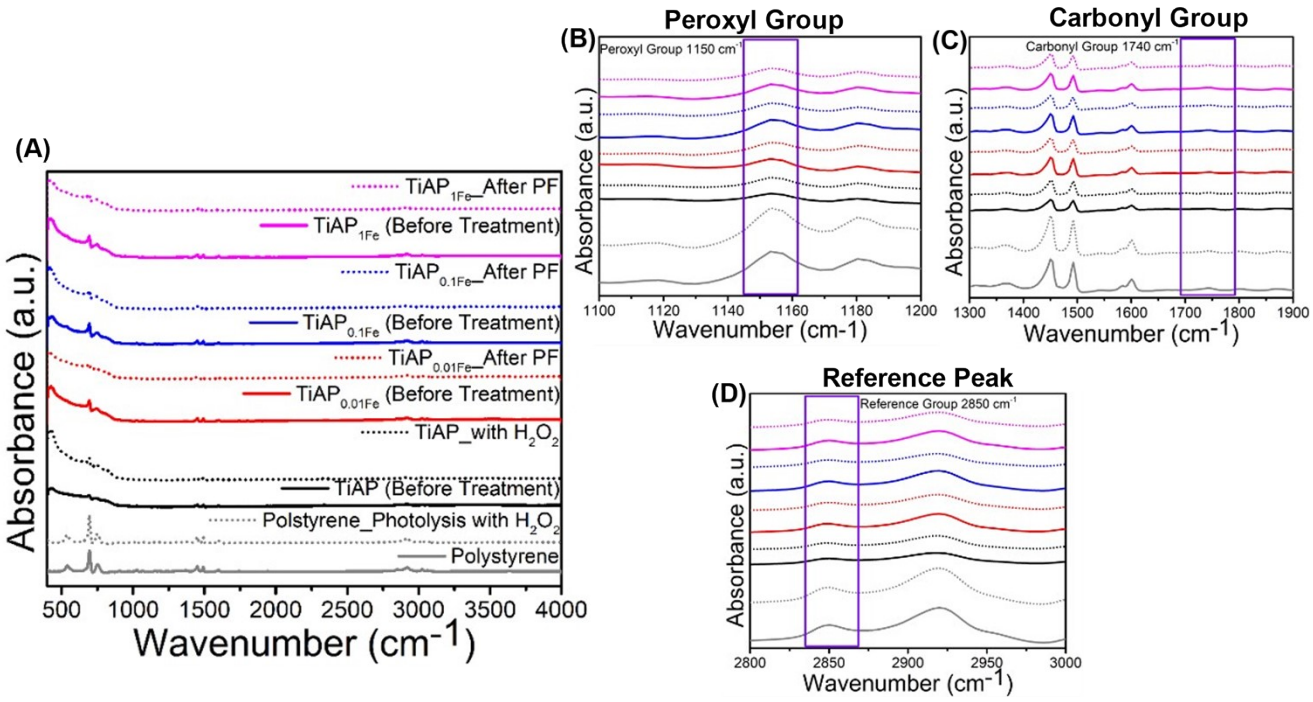

Figure S5: (A) Changes in ATR-IR spectra before (0 min) and after (480 min) the photo-Fenton (PF) process for the TiAP and different concentrations of iron-modified TiAP. On the right side, zoomed-in spectra of the peroxyl group (B), carbonyl group (C), and reference group (D), respectively.

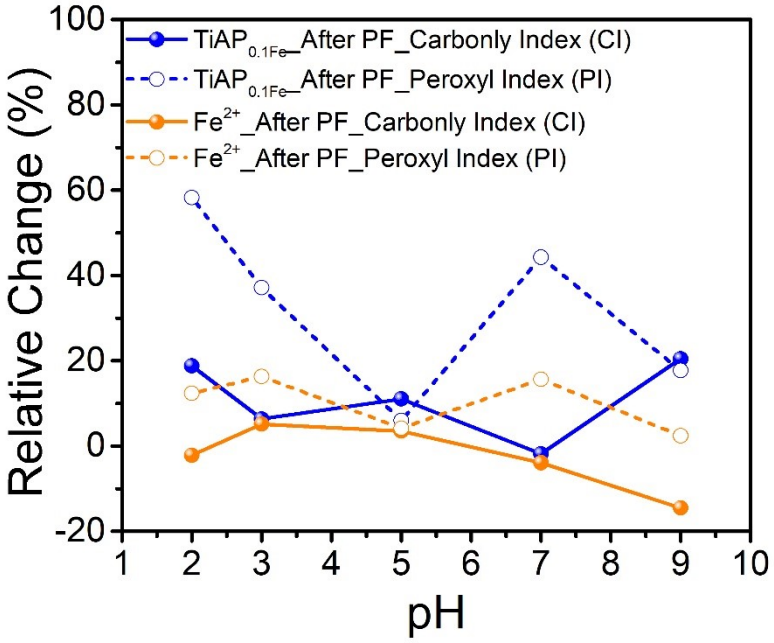

Figure S6: Relative changes in the CI and PI value after the photo-Fenton (PF)-based process for $TiAP_{0.1Fe}$ and homogenous PF process using Fe^{2+} at different pH ranges.

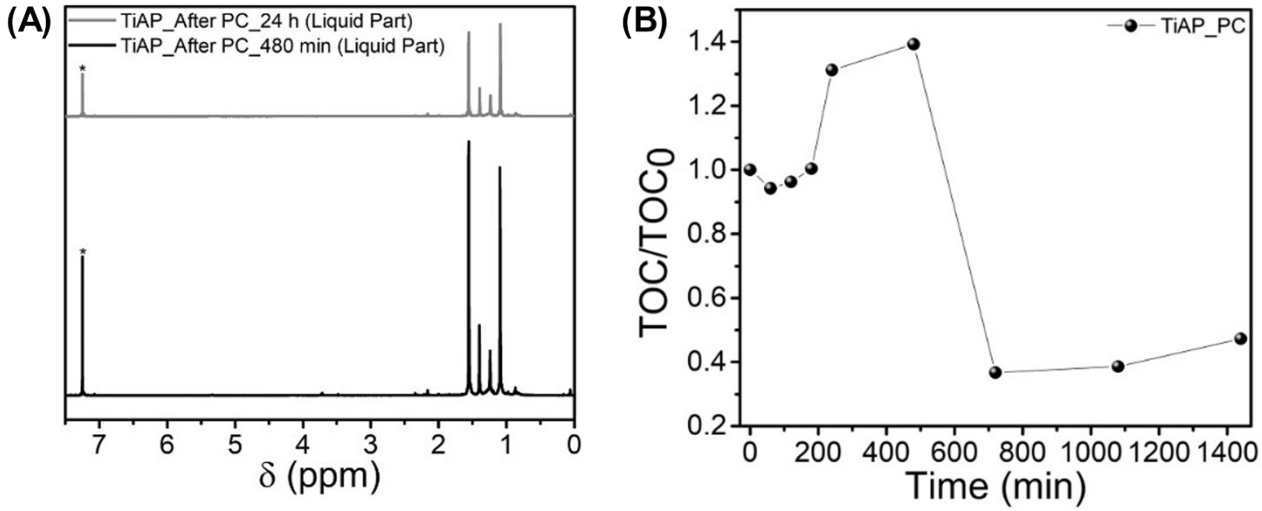

Figure S7: (A) ^{1}H NMR spectra of non-modified TiAP after 480 min and 24 h of photocatalytic (PC) process. Solvent peaks are marked with an asterisk (*). (B) TOC taken after 24 h of PC degradation of PS MPs using non-modified TiAP.

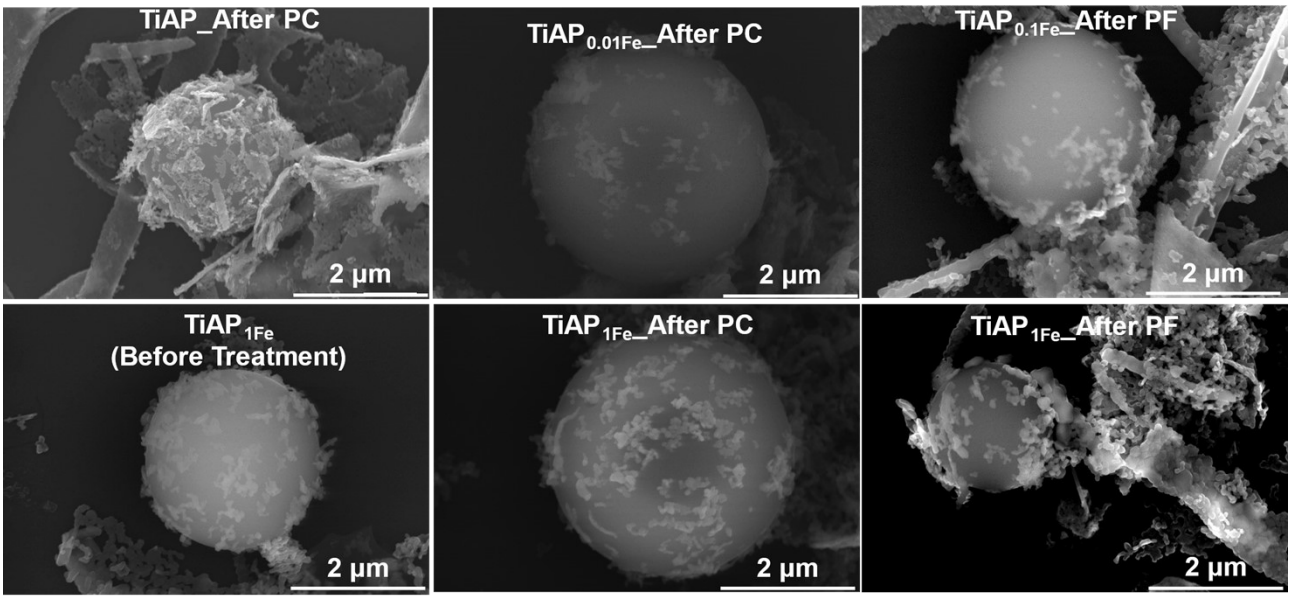

Figure S8: Representative HR-SEM images of samples with a lower change in CI value after photo-induced treatment processes

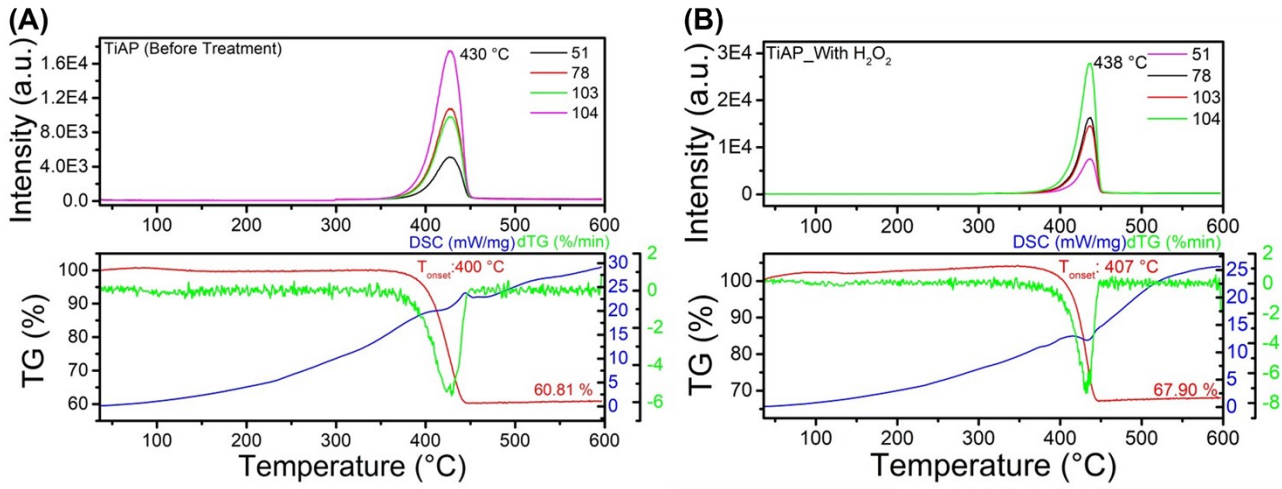

Figure S9: TGA/DSC-MS curves of non-modified TiAP before (A) and after (B) the addition of H_2O_2 for the degradation of PS MPs.

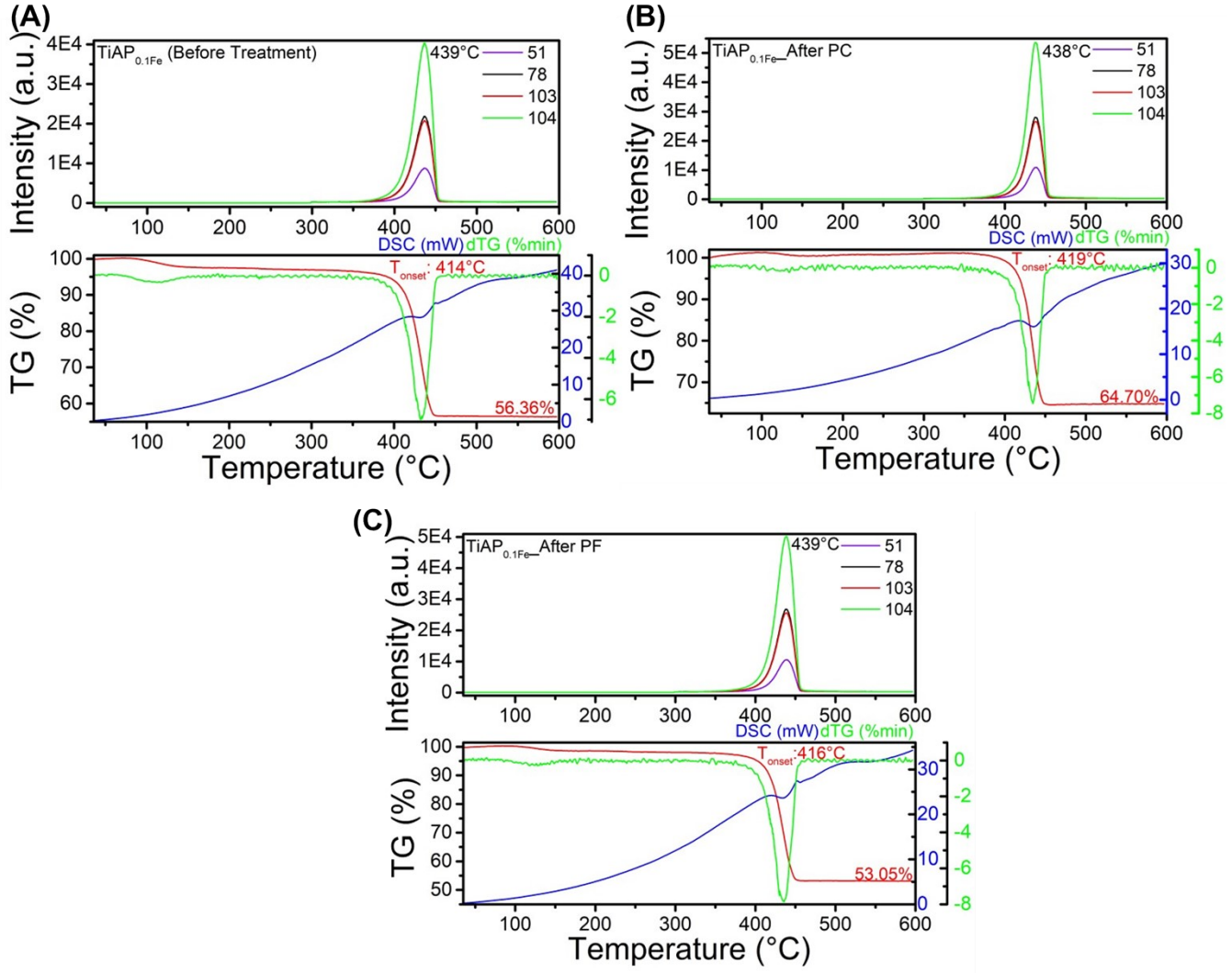

Figure S10: TGA/DTA-MS curves of $TiAP_{0.1Fe}$ before (A) and after the photocatalytic (PC) (B) and photo-Fenton (PF)-based (C) degradation of PS MPs.

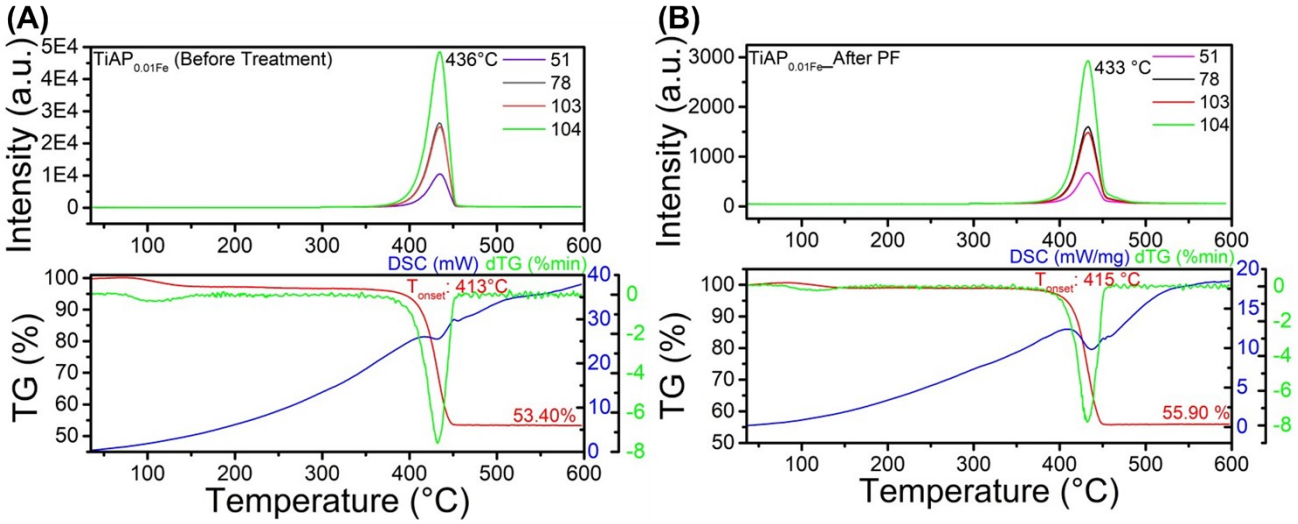

Figure S11: TGA/DSC-MS curves of $TiAP_{0.01Fe}$ before (a) and after (b) the photo-Fenton (PF)-based degradation of PS MPs.

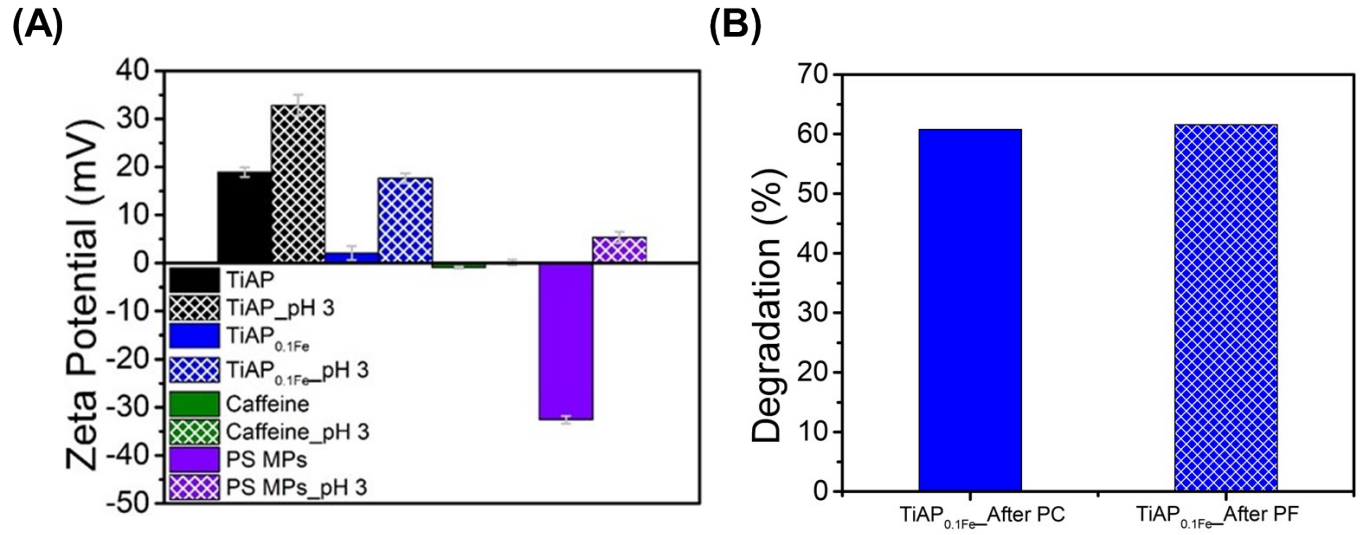

Figure S12: (A) Zeta potential measurements of TiAP, $TiAP_{0.1Fe}$, caffeine, and PS MPs at near neutral pH and acidic pH (~3), respectively. (B) Methylene blue (MB) degradation using $TiAP_{0.1Fe}$ after the photocatalytic (PC) and photo-Fenton (PF) process (photocatalyst: 0.2 mg/mL, reaction volume: 30 mL, MB: 20 ppm, pH 3 and PF process: pH 3, 0.1 mM H_2O_2, irradiation time: 2 h).

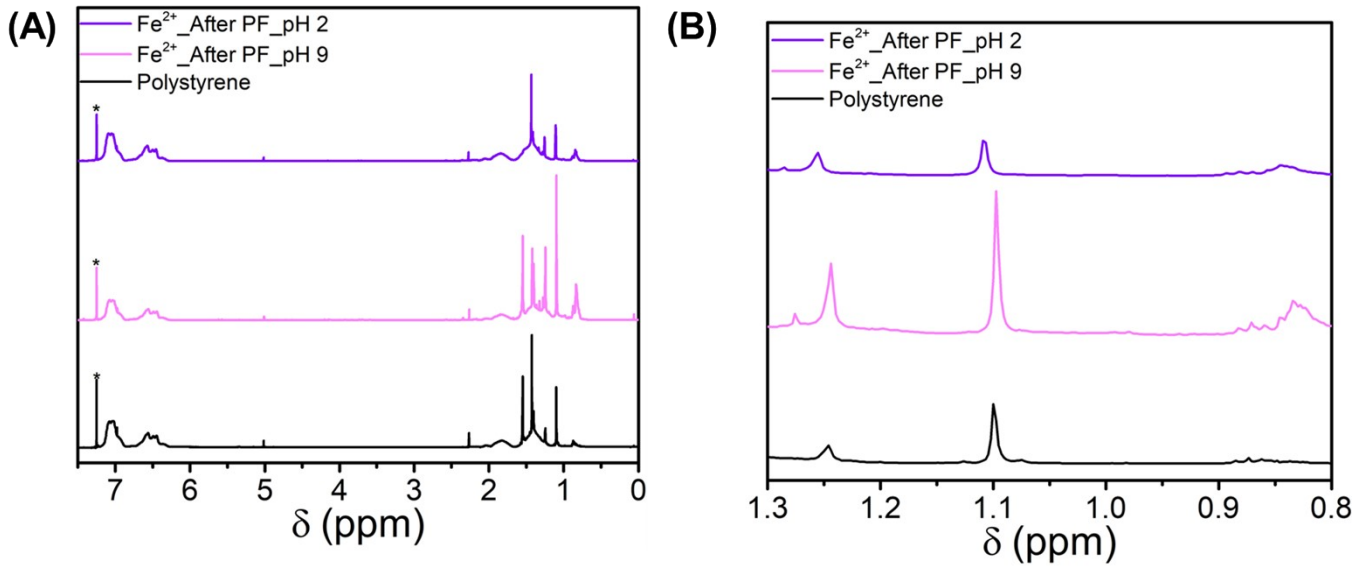

Figure S13: (A) ^{1}H NMR spectra of homogenous photo-Fenton (PF) process using Fe^{2+} salts and (B) the zoomed-in spectra between 0.8-1.3 ppm. Solvent peaks are marked with an asterisk (*).

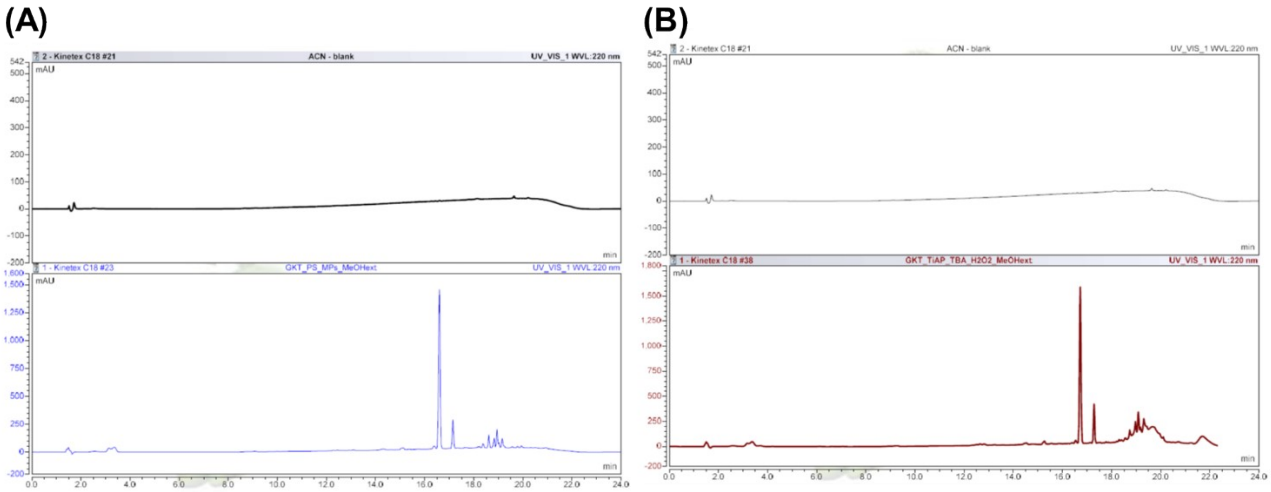

Figure S14: HPLC chromatogram of blank vs PS MPs and TiAP_With H_2O_2 at the wavelength of 220 nm.

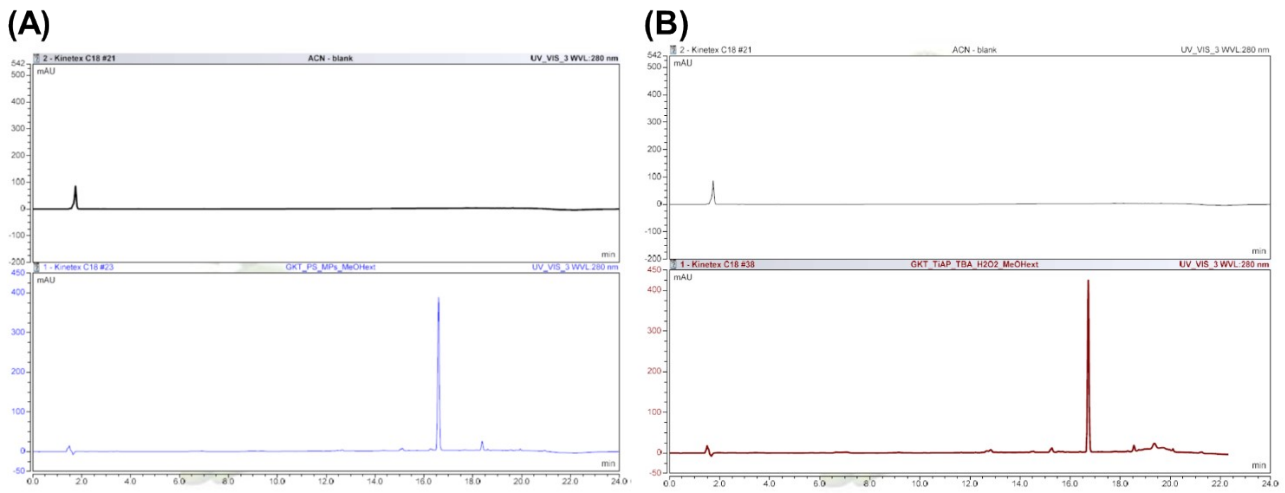

Figure S15: HPLC chromatogram of blank vs PS MPs and TiAP_With H_2O_2 at the wavelength of 280 nm.

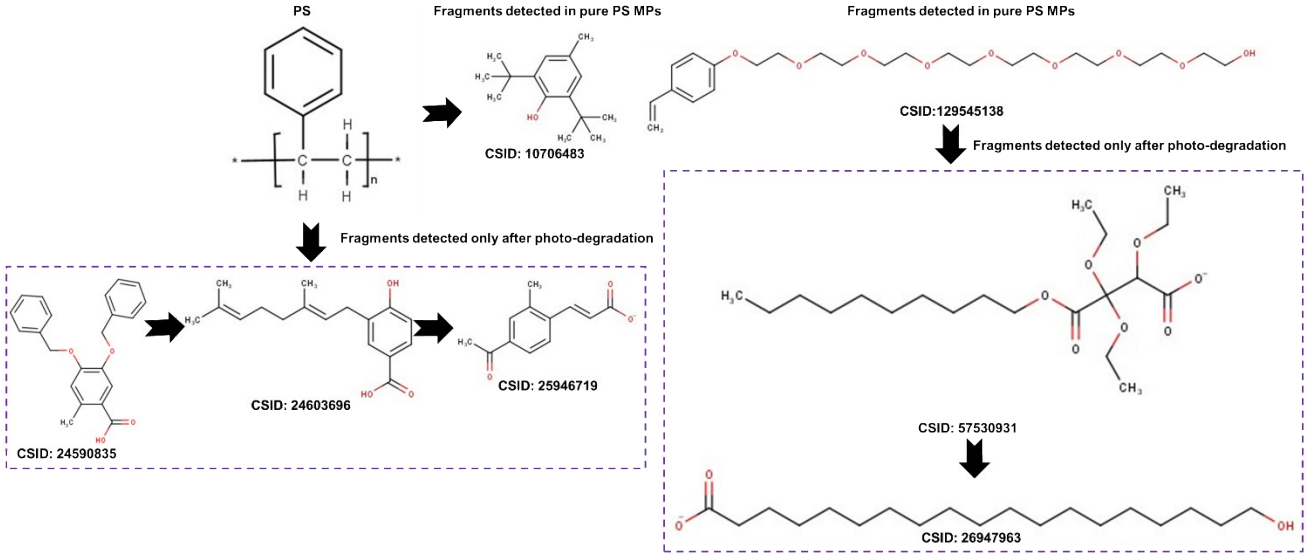

Figure S16: Based on the HPLC-HRMS data, possible intermediates formed during polystyrene degradation were identified. Structures were predicted through https://www.chemspider.com/search. Marvin was used to draw the chemical structures of PS and their intermediates, Marvin 17.21.0, Chemaxon (https://www.chemaxon.com).

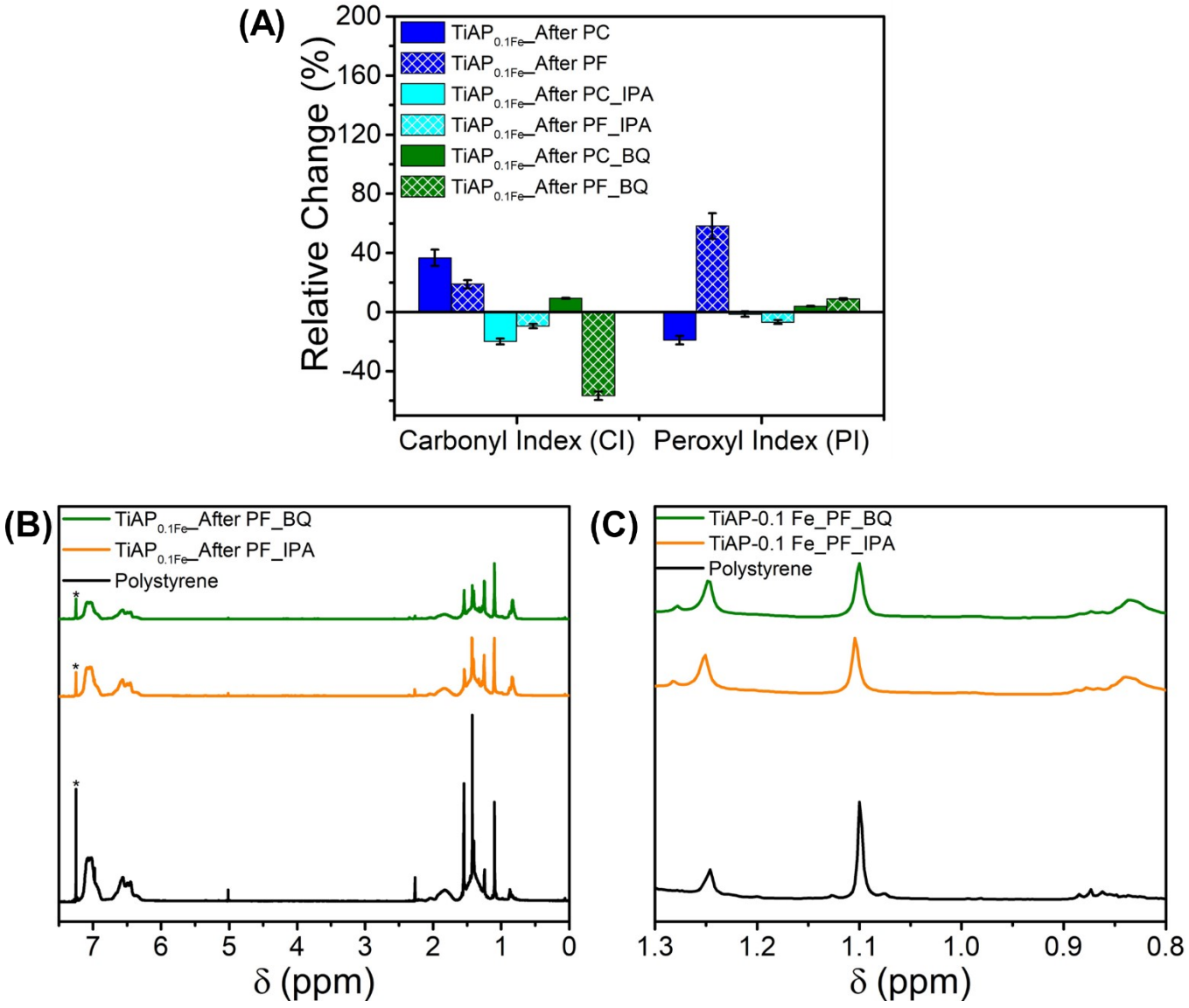

Figure S17: (A) Relative changes in the CI and PI and (B) ^{1}H NMR spectra after the photocatalytic (PC) and photo-Fenton (PF)-based process for $TiAP_{0.1Fe}$ with the addition of isopropyl alcohol (500 mM) and p-benzoquinone (5 mM) as a scavenger. (C) The zoomed-in ^{1}H NMR spectra between 0.8-1.3 ppm. Solvent peaks are marked with an asterisk (*).

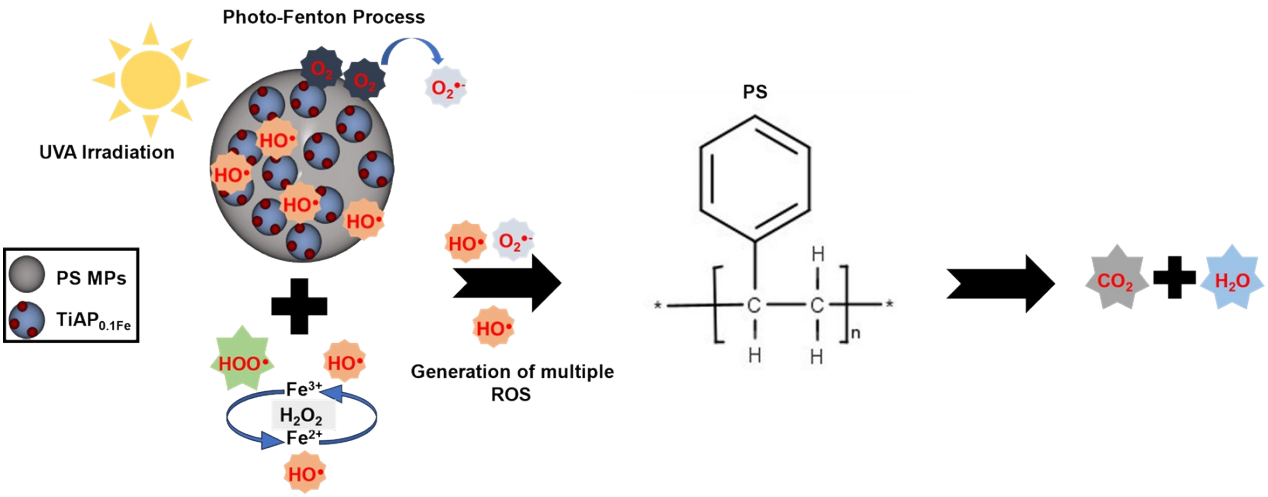

Figure S18: Mechanism of photo-Fenton process in degrading PS MPs using $TiAP_{0.1Fe}$.

Reference

1 J. R. Harbour, J. Tromp and M. L. Hair, Photogeneration of hydrogen peroxide in aqueous TiO_2 dispersions, *Can. J. Chem.*, 1985, **63**, 204–208.

2 P. García-Muñoz, P. H. Allé, C. Bertoloni, A. Torres, M. U. De La Orden, J. M. Urreaga, M.-A. Dziurla, F. Fresno, D. Robert and N. Keller, Photocatalytic degradation of polystyrene nanoplastics in water. A methodological study, *Journal of Environmental Chemical Engineering*, 2022, **10**, 108195.

3 L. P. Domínguez-Jaimes, E. I. Cedillo-González, E. Luévano-Hipólito, J. D. Acuña-Bedoya and J. M. Hernández-López, Degradation of primary nanoplastics by photocatalysis using different anodized TiO2 structures, *Journal of Hazardous Materials*, 2021, **413**, 125452.

4 J. He, L. Han, W. Ma, L. Chen, C. Ma, C. Xu and Z. Yang, Efficient photodegradation of polystyrene microplastics integrated with hydrogen evolution: Uncovering degradation pathways, *iScience*, 2023, **26**, 106833.

5 K. Khairudin, N. F. Abu Bakar and M. S. Osman, Magnetically recyclable flake-like BiOI-Fe3O4 microswimmers for fast and efficient degradation of microplastics, *Journal of Environmental Chemical Engineering*, 2022, **10**, 108275.

6 T. J. Kemp and R. A. McIntyre, Influence of transition metal-doped titanium(IV) dioxide on the photodegradation of polystyrene, *Polymer Degradation and Stability*, 2006, **91**, 3010–3019.